Astrophysical results from COAST

John S. Young, John E. Baldwin, Alastair G. Basden, Nazim Ali Bharmal, David F. Buscher, Amanda V. George, Christopher A. Haniff, James W. Keen, Bridget O'Donovan, Debbie Pearson, Hrobjartur Thorsteinsson, Nathalie Thureau, Robert N. Tubbs, and Peter J. Warner

University of Cambridge, Astrophysics Group, Cavendish Laboratory, Madingley Road, Cambridge CB3 0HE, UK

ABSTRACT

The first-generation COAST array is now primarily operated as a tool for astrophysics, with any development work aimed at improving observing efficiency and at prototyping hardware for future arrays. In this paper we summarise the full range of astrophysical results obtained with COAST in the previous two years. Results of a programme to investigate hotspots on red supergiant stars are presented in detail.

Keywords: Closure phase, hotspots, supergiants, symbiotic stars, Be stars, limb-darkening

1. LATEST RESULTS

The full five-telescope COAST array has been in operation since mid-1998, and has been used for a variety of astrophysical programmes. These include measurements of diameter changes and limb-darkening of Mira variables, observations of binary stars, investigations of hotspots and limb-darkening in supergiants, imaging of the hydrogen envelopes of Be stars, and imaging of symbiotic stars.

There is insufficient space to describe the latest results from all of these programmes in detail here. Therefore we have chosen to present an in-depth treatment of one topic that makes use of the imaging capability of COAST, that of hotspots on late-type supergiants. This treatment is given in Sec. 2, in which our latest results on α Herculis are described. In this section we highlight recent results from our other programmes.

1.1. Symbiotic stars

Preliminary results from our programme on the symbiotic star CH Cygni were reported previously.[1] We have since secured data during 2000 and 2001, to complement the original data from 1999. As the nine-milliarcsecond resolution images in Fig. 1 show, the asymmetry detected in 1999 has persisted. We do not detect the purported second red giant proposed by Skopal and co-workers.[2]

There is clear evidence that the observed disc (assumed to be that of the primary red giant) is asymmetric. The significant improvements in reduced χ^2 in going from a circularly-symmetric to an elliptical disc model are shown in Tab. 1. There is some evidence from the best-fit position angle values that the extension is rotating with period $\sim 15\,\mathrm{yr}$, but further measurements are needed to confirm this.

No further measurements were secured in 2002, as the array was configured for other projects (in particular the supergiant programme described in Sec. 2). We expect to publish a full account of the measurements obtained thus far.

1.2. Be star envelopes

We have secured images in $H\alpha$ of the circumstellar envelopes of γ Cassiopeiae and ζ Tauri, at two different epochs (an image of ζ Tau from 2001 January is shown in Fig. 2). The data include the first closure phase measurements in $H\alpha$ for these stars, and so provide constraints on the apparent symmetry of their hydrogen envelopes. More details of the measurements will be available in Ref. 3.

Further author information:
J.S.Y. (correspondence): E-mail: jsy1001@cam.ac.uk
COAST world-wide-web pages: http://www.mrao.cam.ac.uk/telescopes/coast/

Table 1. Results of fitting Gaussian disc models to the 905 nm visibility amplitude measurements on CH Cyg. Each data-set consists of about 60 independent points. Elliptical disc models with axial ratio ~ 0.8 fit better than circular discs in each case.

Data-set	Red. χ^2	Maj. axis /mas	Axial ratio	Maj. axis PA /°
1999 Aug/Sep	3.3	6.2 ± 0.1	1.0	–
	2.0	6.7 ± 0.1	0.75 ± 0.04	135 ± 4
2000 Jun/Jul/Aug	3.6	6.1 ± 0.1	1.0	–
	3.2	6.2 ± 0.1	0.84 ± 0.06	161 ± 7
2001 Jun/Jul/Aug/Sep	4.1	6.7 ± 0.1	1.0	–
	3.1	7.1 ± 0.1	0.87 ± 0.03	176 ± 10

1.3. Stellar limb-darkening

In addition to limb-darkening measurements for Mira variables, not mentioned here, we have obtained visibility measurements up to the second null for the red giant α Bootis (Fig. 3). The data were secured between 2000 March 21 and 2000 April 10. The waveband for the measurements was centred on 905 nm, with FWHM 50 nm. A full account of these measurements is in preparation.

2. HOTSPOTS ON SUPERGIANT STARS

The primary aim of the ongoing COAST programme on red supergiants is to test and refine the model for hotspot formation proposed by Young et al.[4] In this model, the large hotspots seen at optical wavelengths correspond to areas of elevated temperature in the stellar photosphere, whose apparent contrast with the surrounding disc is enhanced by a local reduction in opacity. The locally raised temperatures, and corresponding reduction in molecular opacity, are most likely due to convection — this offers a convenient explanation for changing hotspot locations and brightnesses.

Young et al. used a simple blackbody parametrization of this model to fit multi-wavelength data on α Orionis. The hotspots were represented by unobscured areas at a given temperature, and the wavelength-dependent opacity obscuring the remaining parts of the stellar disc was modelled by allowing the disc angular diameter and temperature to vary as a function of observing wavelength.

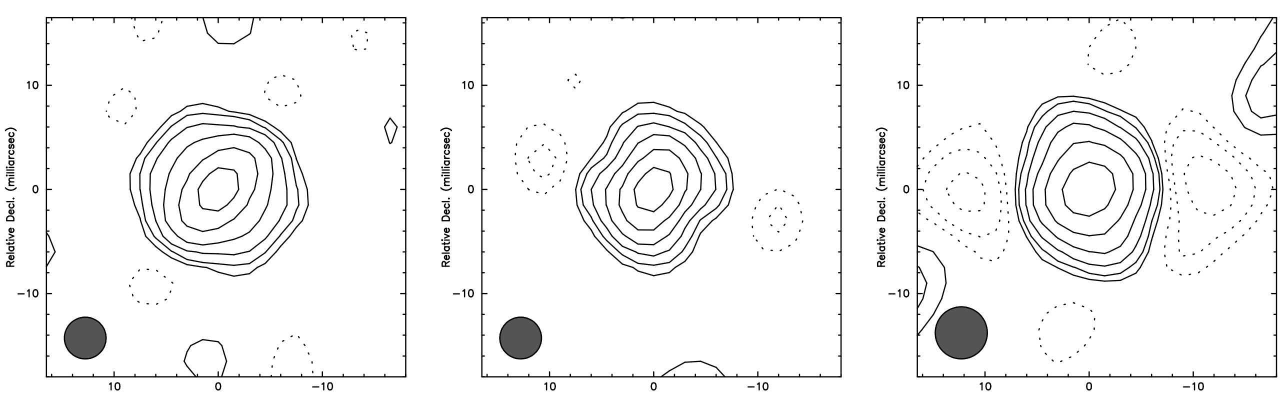

Figure 1. 905 nm-wavelength images of the symbiotic star CH Cyg. The maps were reconstructed using the standard self-calibration/CLEAN procedure used in radio astronomy. Contours are plotted at -8, -4, -2, 2, 4, 8, 16, 32, and 64 per cent of the peak flux.

The opacity-enhanced model for hotspots leads to two predictions:

- Large changes in hotspot contrast should be seen when crossing deep spectral features
- Temporal variations in hotspot contrast and TiO band strength should be correlated

For the 2002 observing season, we planned to test the first prediction, by making simultaneous imaging observations using narrow ($\sim 5\,$nm) bandpasses in both strong TiO absorption features and the nearby continuum. The two brightest northern supergiants, α Orionis (M2Iab) and α Herculis (M5II), were selected as targets (only data on α Her is presented here). To match the angular resolution of the observations with the expected size of the stellar discs and hotspots, three of the COAST telescopes were arranged in the most compact configuration possible, with a maximum baseline of six metres.

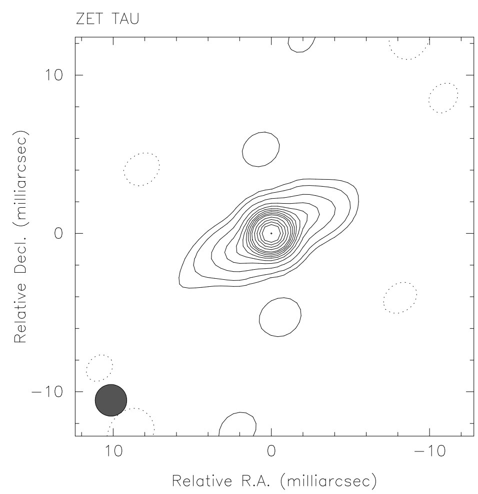

Figure 2. Reconstructed image of ζ Tau in $H\alpha$, from 2001 January. Contours are plotted at -1, 1, 2, 5, 10, 15, 20, 25, 30, 35, 40, 50, 60, 70, 80, 90, and 99 per cent of the peak flux.

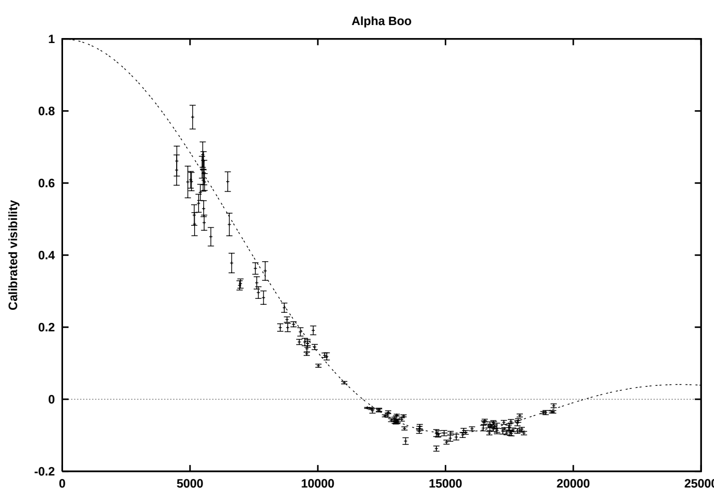

Figure 3. Visibility measurements at 905 nm for α Boo. In the case of a symmetric disc, the complex visibility is purely real, and its sign can be inferred from closure phase measurements. The signs of the plotted points were determined in this manner.

Table 2. Log of COAST observations of α Her. Dates refer to the start of each night. N_{vis} and N_{cl} give the number of successful visibility and closure-phase measurements made. Each "measurement" corresponds to 60–200 seconds of data, in one or more colours simultaneously.

Date(s)	Baseline range /m	N_{vis}	N_{cl}	[λ/nm] / [$\Delta\lambda$/nm]
2002/03/27	2.1	2	–	782/5 750/13
2002/03/28	2.3–5.6	17	4	782/5 750/13
2002/03/29	2.5–6.0	11	4	782/5 750/13
2002/04/03	2.6–4.7	3	2	782/5 750/13
2002/04/04	2.5–5.7	12	5	782/5 750/13
2002/04/16	2.7–6.0	20	5	782/5 750/13
1996/04/01	2.8–7.9	14	10	940/60 905/50 880/11
1996/04/03	2.2–8.5	22	11	940/60 905/50
1996/05/04	3.0–8.5	9	7	940/60 905/50 830/40 750/13
1996/05/05	2.6–8.4	9	12	940/60 800/11 750/13
1996/05/06	2.6–8.5	25	10	940/60 905/50
1996/05/07	2.0–7.3	20	7	940/60 905/50
1996/05/20	3.0–8.2	7	–	940/60 830/40
1996/06/14	4.0–8.4	9	4	940/60
1996/06/24	4.0–8.4	17	8	940/60 800/11 780/30

Archive data from 1996 was also found to be useful in testing the model predictions. The measurements are described in more detail below.

2.1. Observations and data reduction

2.1.1. Observations in 2002

α Her was observed on six nights during March and April 2002, using three of the COAST telescopes, which were arranged in a compact configuration (foundations C W2 E1). Standard observing procedures were employed, including interleaving of fringe measurements on α Her and measurements on an unresolved calibrator star (α Ophiuchi).

The visible ($\lambda < 1\mu$m) beam-combiner was used, with the observing wavebands selected using filters mounted in front of the four avalanche photodiode (APD) detectors. Filters centred on 782 nm with 5 nm half-power bandwidth were used with two of the APDs, and a 750/13 nm filter with the third (continuum filters can be slightly wider, as the effective bandpass is flux-weighted). A broad (30 nm) filter centred on 780 nm was used with the fourth APD, to give a high signal-to-noise channel for fringe finding. The 40 cm COAST siderostats were typically stopped down to 16 cm ($\sim 2.5r_0$), to match the seeing conditions.

Data were recorded using each of the three sub-array baselines in turn, followed by one or more recordings of fringes on all three baselines simultaneously to measure the closure phase. This sequence was repeated for the calibrator star, before returning to the target. The number of measurements of visibility amplitude and closure phase made on each night are given in Tab. 2. Each recording was of length 60–200 s, to fully sample the visibility fluctuations caused by the atmosphere, and to ensure adequate signal-to-noise.

2.1.2. Observations in 1996

The observing procedure used in 1996 differed only in detail. The filters used with the four APDs varied from night to night (and were sometimes changed during the night) — details are given in Tab. 2. At the time of the observations only three COAST telescopes were operational, and these were laid out in a slightly larger (C W3 E1) configuration than that used in 2002. Table 2 gives the range of projected baselines obtained on each night.

2.1.3. Data reduction

All of the data were reduced using the same standard techniques. These techniques are described in more detail in Refs. 5 and 6. Squared visibility amplitudes were estimated from the single-baseline data by averaging the power spectra of scans through the fringe envelope, and estimating the fringe power by integrating over the noise-subtracted fringe peak.

Uncertainties in these uncalibrated squared amplitudes were estimated from the scatter in values obtained from different segments of the same recording, and hence include contributions from visibility fluctuations during the recording and from photon noise. The squared amplitudes were calibrated by dividing them by the system squared visibility, obtained from an adjacent measurement of the calibrator star. Additional uncertainties (five or ten per cent of the amplitude) were added in quadrature, to account for potential changes in seeing between the observations of target and calibrator.

Closure phases were estimated from the three-baseline data, by dividing the data into “coherent intervals” of duration $\sim 2t_0$, and estimating the bispectrum from each interval. The complex bispectrum estimates were summed over the recording, the phase of the resultant being the adopted closure phase value. The error in the closure phase was calculated from the scatter in the interval estimates projected perpendicular to the mean bispectrum vector. Uncertainties on the final closure phases were in the range 5–20 degrees.

2.2. Results

2.2.1. Analysis procedure

We have followed very similar procedures to those described in Ref. 4, except that here the Fourier plane coverage was always insufficient to allow model-independent image reconstructions. Hence we have relied solely on fitting relatively simple parametrizations of the sky brightness distribution to the visibility amplitudes and closure phases measured at a particular wavelength and epoch.

The parametrizations consisted of a limb-darkened disc (using the empirical model of Hestroffer[7]) plus some number of smaller disc components, representing superimposed bright spots. A conjugate-gradient algorithm was used to find the model parameters that minimized χ^2, using a range of starting conditions to improve the chance of identifying a global minimum. Uncertainties in the best-fitting parameters were estimated from the curvatures of the χ^2 hyper-surfaces around minima, having accommodated any correlations between the different parameters.

2.2.2. Evidence for asymmetries in 2002

The 2002 data considered here were obtained over a period of 20 days. Changes in surface morphology on a timescale of three weeks are typically small.[8] Hence, after checking for consistency between nights as far as possible, all of the 2002 data in a particular waveband were combined for the analysis described here.

The visibility amplitudes at both 782 nm (Fig. 4) and 750 nm are consistent with a uniform disc model (and hence with any reasonable limb-darkened model) on baselines shorter than about $7\,\mathrm{M}\lambda$. Beyond this projected baseline, there is an excess of visibility compared with the prediction of the simple model.

The closure phase data are also shown in Fig. 4. At both wavelengths, the closure phase is small ($< 20^\circ$) when the projected baselines making up the triangle are all shorter than $6.8\,\mathrm{M}\lambda$, and somewhat larger (up to $\sim 70^\circ$ at 782 nm; up to $\sim 50^\circ$ at 750 nm) when the longest projected baseline exceeds this length. Closure phase values inconsistent with zero or 180° are unambiguous evidence of asymmetry. Centro-symmetric models were unable to fit the data, the lowest reduced χ^2 value obtained for the 782 nm data being 6.9.

The Fourier coverage of the data is insufficient to unambiguously determine the nature of the asymmetry. However, adequate fits ($\chi^2 \approx 2$) were obtained by modelling the flux distribution as a limb-darkened disc plus a single superimposed bright feature. The parameters of this model could be determined unambiguously for both colours: the best-fit radial coordinate of the “hotspot” was the same in both cases, and the values for its position angle were marginally consistent (being $119 \pm 22^\circ$ at 782 nm and $157 \pm 19^\circ$ at 750 nm). The fit obtained at 750 nm by fixing the hotspot in the 782 nm location was not significantly worse, hence the hotspots were assumed to be coincident for the subsequent analysis.

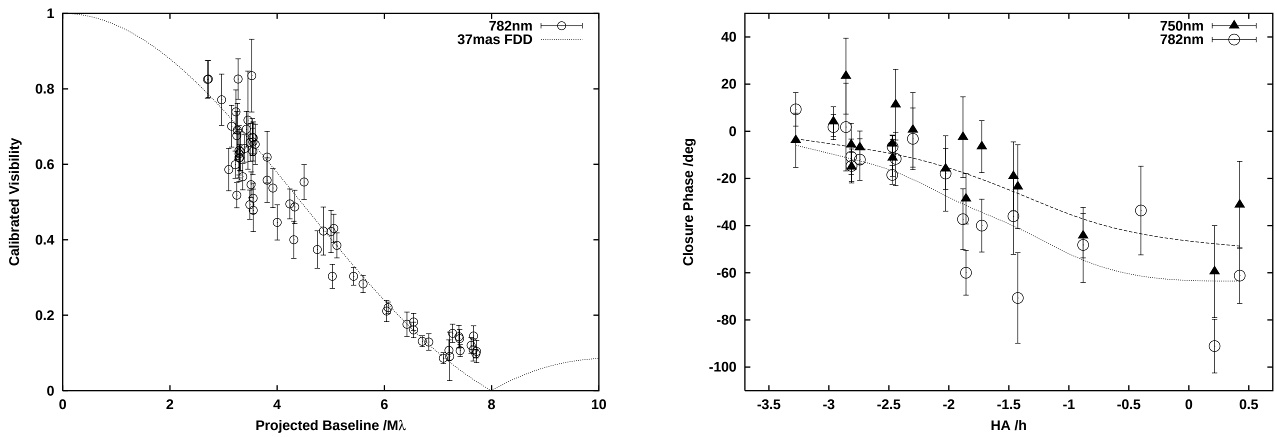

Figure 4. Visibility amplitudes at 782 nm for α Her in 2002 (left panel), and closure phase values at both 782 and 750 nm (right panel). The predictions of the appropriate models from Tab. 3 are also shown in the right-hand panel.

The Hestroffer limb-darkening parameter α is hardly constrained by the 2002 data — discs with α in the range 0–4 are practically indistinguishable on the baselines measured. A value of unity was adopted (this model is abbreviated to "FDD" — for Fully-Darkened Disc — in some of the figures). The size of the hotspot is also indeterminate. Results are presented for moderately-resolved hotspots (Gaussian FWHM of 10 mas), for consistency with the 1996 results below.

2.2.3. Evidence for asymmetries in 1996

The entire 1996 data-set spans 84 days. Significant changes would certainly be expected over this period. In fact different sub-sets of the wavebands were used on different nights, so only the timespans for 940, 905, and 800 nm exceed the typical hotspot evolution time of 20 days.[8] The 905 nm closure phase values from April are not consistent with those from May, whereas all of the 940 and 800 nm data is self-consistent.

As the number of data points in some wavebands is barely sufficient to constrain the surface structure, all of the data in a particular waveband were combined for model-fitting, except at 905 nm where only the data from May were considered. Mean dates for each waveband are given in Tab. 3, and the reader should bear in mind that those for 880 nm and 780 nm differ significantly from the dates for the other five wavebands. Changes occurring within the timespan of the data-set at a particular wavelength could also lead to badly-fitting models compared with single-epoch data.

The 940 nm data-set, being the largest, gives the best constraints on the flux distribution. The closure phases are obviously not consistent with zero or 180° (Fig. 6) — the best χ^2 obtained for a symmetric disc model was 6.9 ($\chi^2 = 20$ for the closure phases alone) for a Hestroffer disc with $\alpha = 2$. Adding a single hotspot could significantly improve the χ^2 (to ~ 5 for the closure phases, ~ 3 overall), provided the hotspot was resolved (Gaussian FWHM ≥ 10 mas). This is necessary to fit the small visibilities close to the "null" (Fig. 5), while still reproducing the closure phase signature (Fig. 6).

Non-zero closure phases were also measured at the other wavelengths, bar 880 nm. Only the 940 nm data could constrain both the radial and azimuthal coordinates of the hotspot (with a prior forcing it to be on the disc — hotspots were modelled as sharp-edged discs to facilitate the application of this condition). Assuming the position angle from the 940 nm data, the 750 nm data could unambiguously constrain the radius of the hotspot. The 905 nm data could constrain the position angle but not the radius. Importantly, in no case was it possible to fit a data-set with a much brighter or fainter hotspot than that given in Tab. 3.

To investigate the wavelength-dependence of the hotspot flux, we have assumed its location to be independent of wavelength. The data do not contradict this assumption, and it has been found to be generally true for supergiants on previous occasions when hotspots have been detected at multiple wavelengths.[4, 9–11]

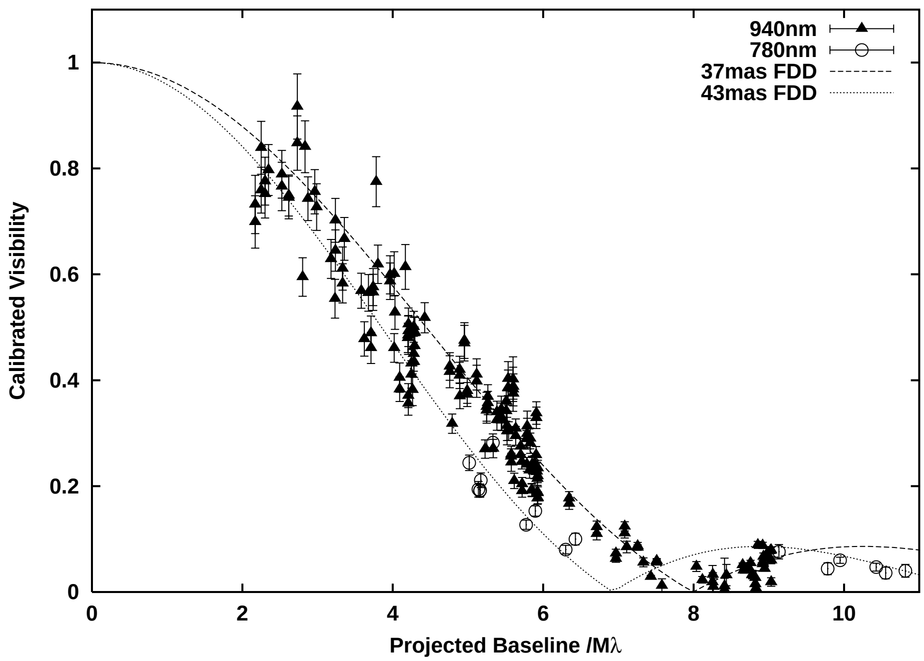

Figure 5. Visibility amplitudes at 940 nm (solid triangles) and 780 nm (open circles), illustrating that at the time of the 1996 observations, α Her was significantly more resolved in the light of the TiO band at 780 nm.

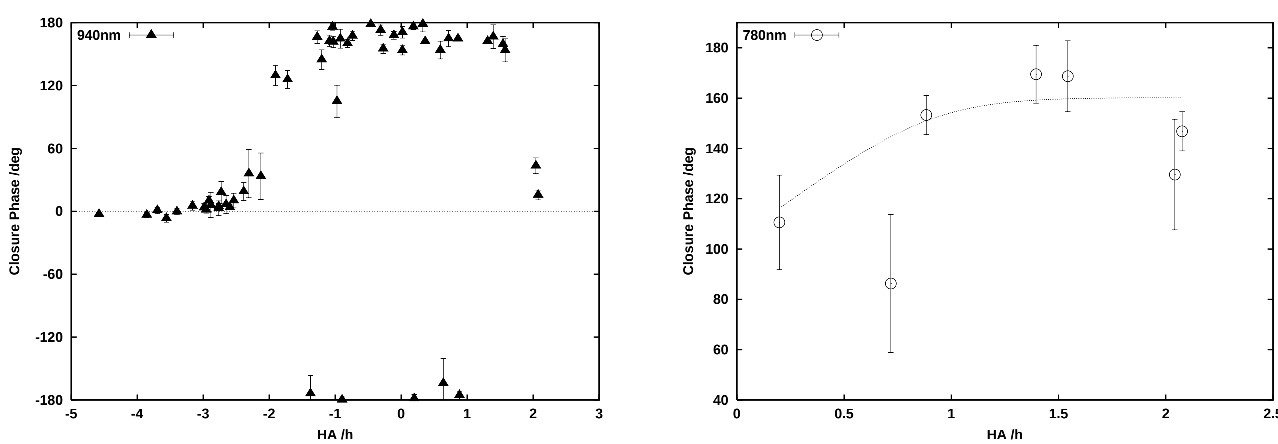

Figure 6. Closure phases at 940 nm (left panel) and at 780 nm (right panel). The dotted curve in the right-hand panel corresponds to the model for 780 nm from Tab. 3.

Table 3. Results of fitting models with fixed hotspot locations (obtained from the 782 nm data for 2002, and the 940 nm data for 1996). The adopted hotspot locations are given in the last two columns. Refer to the text for details. The dates correspond to the mean of the Julian days on which measurements were made in the given waveband. Hotspots were modelled as Gaussians with 10 mas FWHM (2002 data), or Hestroffer discs with diameter 18 mas and limb-darkening parameter $\alpha = 1$ (1996 data).

Year	Mean date	λ/nm	Red. χ^2	FDD diam. /mas	Frac. hotspot flux	r/mas	θ/mas
2002	04/02	782	2.4	37.4 ± 0.7	$.19 \pm .01$	8($\pm$5)	114($\pm$19)
	04/02	750	1.9	33.9 ± 0.5	$.13 \pm .02$		
1996	05/10	940	3.3	37.5 ± 0.1	$.018 \pm .001$	11($\pm$2)	199($\pm$6)
	05/06	905	3.8	36.9 ± 0.2	$.019 \pm .005$		
	04/01	880	1.0	38.4 ± 0.7	$< .05$		
	05/12	830	0.9	37.6 ± 0.3	$.053 \pm .004$		
	05/05	800	2.5	37.7 ± 0.4	$.074 \pm .006$		
	06/24	780	3.2	42.6 ± 0.4	$.030 \pm .008$		
	05/05	750	1.8	36.9 ± 0.5	$.065 \pm .009$		

A model with the hotspot fixed in the location obtained from the 940 nm data was fit to each waveband separately. The flux of the hotspot and the disc size were allowed to vary. The resulting best-fit parameters are given in Tab. 3. We chose a value of unity for the limb-darkening parameter α for these final model-fits. Similarly acceptable fits to the 1996 data can be obtained with $\alpha = 2$, but the hotspot fluxes are not changed significantly.

2.2.4. Wavelength dependence

The results of fitting single-hotspot models to the 2002 data (Tab. 3) show that the contrast between hotspot and disc is significantly enhanced in the TiO band at 782 nm, compared with the 750 nm continuum. The stellar disc is also 10 per cent larger at 782 nm.

The wavelength-dependence of the hotspot flux (quoted as a fraction of the total flux in the model) in 1996 is plotted in Fig. 7. Here the behaviour is opposite to that seen in 2002 — the hotspot is *weaker* in the TiO-contaminated band. However, some of the apparent wavelength-dependence may be attributable to temporal changes: the effective epoch of the 780 nm measurement is the latest of all the colours.

If the point at 780 nm is neglected, a general trend of decreasing hotspot flux with increasing wavelength is seen. This is similar to the trend observed over a larger wavelength range by Young et al.[4] The disc diameter is constant with wavelength, except at 780 nm, where it is 14 per cent larger.

2.3. Discussion

The comparison between the 1996 and 2002 data is intriguing. The generally larger disc diameters measured in 1996 suggest either a change in the intrinsic size of α Her, or more likely, higher opacities in 1996.

In the limit of extremely high opacity in the outermost photospheric layers, it is clear that any area of enhanced temperature in the deeper photosphere can be completely masked. This kind of behaviour could explain the observation of reduced, rather than enhanced, hotspot contrast in the TiO band. The larger enhancement in disc size in the TiO band in 1996, despite the use of a wider filter, is further evidence for higher opacity at the earlier epoch.

Higher opacities are to be expected in α Her compared with α Ori, due to its later spectral type. This would be consistent with TiO-suppressed hotspots occurring sometimes in α Her, and (perhaps) not at all in Betelgeuse.

In the high-opacity regime, the blackbody parametrization used by Young et al. will not work without modification, as it assumes that the hotspots are unobscured. Quantitative comparison of the new data with the convective picture of hotspot formation is needed, but more appropriate parametrizations are beyond the scope of this paper.

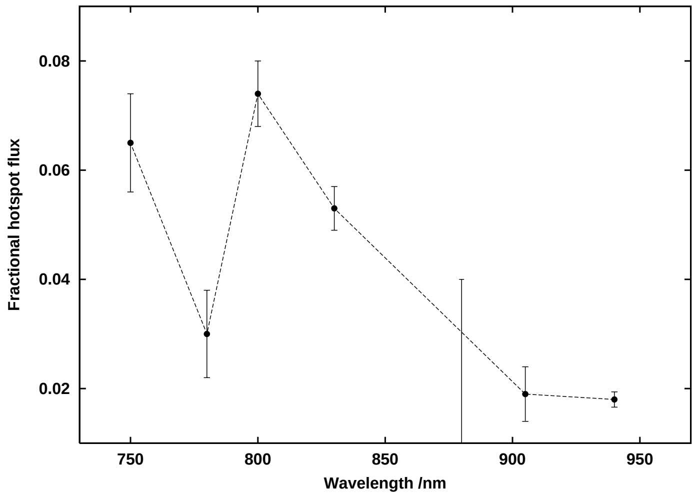

Figure 7. Wavelength-dependence of hotspot flux, as measured in 1996. Only an upper limit was determined at 880 nm.

2.4. Conclusions and future work

The new data provide further evidence that hotspots are ubiquitous on late-type supergiant stars, at least at visible wavelengths. We have identified two types of behaviour in α Her: enhancement of hotspot contrast in a TiO band, and also suppression of hotspot contrast in the same band, at an epoch when the outer atmosphere was probably more opaque.

Further interpretation of these data requires some modelling effort, both to modify the "first-order" blackbody parametrization used previously, and also to compare the data with the predictions of the three-dimensional hydrodynamic models of Freytag (these proceedings, paper 4838-93).

Monitoring of a small sample of the brightest supergiants would be desirable, to measure changes in the wavelength-dependence of the surface structures. Such measurements are best made at frequent (~ 2 week) intervals. Contemporaneous spectrophotometric measurements would give an independent handle on the variations in TiO opacity.

REFERENCES

1. J. S. Young, J. E. Baldwin, R. C. Boysen, A. V. George, C. A. Haniff, C. D. Mackay, D. Pearson, J. Rogers, P. J. Warner, D. M. A. Wilson, and R. W. Wilson, "Recent astronomical results from COAST," in *Interferometry in Optical Astronomy*, P. J. Lena and A. Quirrenbach, eds., *Proc. SPIE* **4006**, pp. 472–479, 2000.
2. A. Skopal, M. F. Bode, H. M. Lloyd, and S. Tamura, "Eclipses in the symbiotic system CH Cyg," *Astron. Astrophys.* **308**, pp. L9–L12, 1996.
3. A. V. George. PhD thesis, University of Cambridge, 2002. In preparation.
4. J. S. Young, J. E. Baldwin, R. C. Boysen, C. A. Haniff, P. R. Lawson, C. D. Mackay, D. Pearson, J. Rogers, D. St.-Jacques, P. J. Warner, D. M. A. Wilson, and R. W. Wilson, "New views of Betelgeuse: multi-wavelength surface imaging and implications for models of hotspot generation," *Mon. Not. R. astr. Soc.* **315**, pp. 635–645, 2000.
5. D. Burns, *Experiments with the Cambridge Optical Aperture Synthesis Telescope*. PhD thesis, University of Cambridge, 1997.
6. D. Burns, J. E. Baldwin, R. C. Boysen, C. A. Haniff, P. R. Lawson, C. D. Mackay, J. Rogers, T. R. Scott, P. J. Warner, D. M. A. Wilson, and J. S. Young, "The surface structure and limb-darkening profile of Betelgeuse," *Mon. Not. R. astr. Soc.* **290**, pp. L11–L16, 1997.

7. D. Hestroffer, “Centre to limb darkening of stars: new model and application to stellar interferometry,” *Astron. Astrophys.* **327**, pp. 199–206, 1997.
8. R. W. Wilson, V. S. Dhillon, and C. A. Haniff, “The changing face of Betelgeuse,” *Mon. Not. R. astr. Soc.* **291**, pp. 819–826, 1997.
9. D. F. Buscher, C. A. Haniff, J. E. Baldwin, and P. J. Warner, “Detection of a bright feature on the surface of Betelgeuse,” *Mon. Not. R. astr. Soc.* **245**(1), pp. 7p–11p, 1990.
10. R. W. Wilson, J. E. Baldwin, D. F. Buscher, and P. J. Warner, “High-resolution imaging of Betelgeuse and Mira,” *Mon. Not. R. astr. Soc.* **257**, pp. 369–376, 1992.
11. P. G. Tuthill, C. A. Haniff, and J. E. Baldwin, “Hotspots on late-type supergiants,” *Mon. Not. R. astr. Soc.* **285**, pp. 529–539, 1997.